Anisotropy effects onmicrostructure and properties in decomposed arc evaporated Ti1-xAlxN coatings during metal cutting

Mats P. Johansson Jöesaar, Niklas Norrby, Jennifer Ullbrand, R. Saoubi and Magnus Odén

Original Publication:

Mats P. Johansson Jöesaar, Niklas Norrby, Jennifer Ullbrand, R. Saoubi and Magnus Odén, Anisotropy effects onmicrostructure and properties in decomposed arc evaporated Ti1-xAlxN coatings during metal cutting, 2013, Surface & Coatings Technology, (235), 25, 181-185.
http://dx.doi.org/10.1016/j.surfcoat.2013.07.031

Surface & Coatings Technology 235 (2013) 181–185

Contents lists available at ScienceDirect

Surface & Coatings Technology

journal homepage: www.elsevier.com/locate/surfcoat

Anisotropy effects on microstructure and properties in decomposed arc evaporated $Ti_{1-x}Al_xN$ coatings during metal cutting

M.P. Johansson Jõesaar [a,b,*], N. Norrby [a], J. Ullbrand [a], R. M'Saoubi [b], M. Odén [a]

[a] Nanostructured Materials, Department of Physics, Chemistry and Biology, IFM, Linköping University, SE-58183 Linköping, Sweden
[b] Seco Tools AB, SE-73782 Fagersta, Sweden

ARTICLE INFO

Article history:
Received 22 March 2013
Accepted in revised form 10 July 2013
Available online 19 July 2013

Keywords:
Cathodic arc evaporation
TiAlN
Anisotropy
Microstructure
Hardness
Metal cutting

ABSTRACT

Anisotropy effects on the spinodal decomposition in cathodic arc evaporated cubic "phase c-$Ti_{1-x}Al_xN$ coatings have been studied with respect to composition, microstructure and hardness properties before and after a continuous turning operation. Coatings are simultaneously being exposed to both a high temperature and high pressure during the metal cutting process. As evident from the current results, a high Al content coating, x = 0.66, when exposed to such extreme conditions decomposes into cubic c-AlN and c-TiN-rich domains. In this case, the evolving microstructure comprises interconnected spatially periodic, elongated and coherent cubic c-AlN and c-TiN-rich regions aligned along elastic compliant <100> crystal direction. A significantly different microstructure with randomly oriented domains is observed for a coating with an elemental composition closer to the isotropic limit, x = 0.28, exposed under the same conditions. From a coating hardness perspective, the nanoindentation results display a minor age hardening effect for the c-$Ti_{1-x}Al_xN$ coating grown at x = 0.28 while the coating grown with x = 0.66 exhibits a significant age-hardening effect of about 18%. We conclude that both microstructure and age hardening behavior during spinodal decomposition of c-$Ti_{1-x}Al_xN$ correlate to the relative amount of metal Ti/Al ratio and consequently to the elastic anisotropy of the as-grown coating material. These results provide new insights to the understanding of improved wear resistance of c-Ti1$_{-x}$AlxN with Al content during metal cutting.

1. Introduction

(Ti,Al)N-based coatings are among the most common hard and protective coating materials used in today's metal cutting applications. The cubic, B1, structure of (Ti,Al)N, as a monolith layer and/or part of a laminated coating structure, combine attractive mechanical properties such as high hardness [1–3] and improved temperature and oxidation resistance [2,4,5] providing good performance in metal machining applications [6,7]. The technological benefits of (Ti,Al)N and its excellent physical properties, especially at elevated temperatures, are partly explained in terms of a spinodal decomposition process during which cubic (Ti,Al)N decomposes isostructurally into coherent cubic c-AlN- and c-TiN-enriched domains [1,3,8,9]. The combination of elastic properties [10] and a lattice mismatch [11] between coherent c-AlN- and c-TiN-enriched domains leads to significant *age hardening* during which the hardness of (Ti,Al)N thin layers has shown to increase with between 15% and 20% [1,5]. Similar *age hardening* in spinodally decomposed cubic systems has earlier been discussed by Cahn [12]. At further aging, c-AlN transforms into the thermodynamically stable hexagonal, wurtzite B4 structure, w-AlN resulting in a dual phase structure comprising c-TiN and w-AlN with reduced mechanical properties [2].

The temperature regime, i.e., at about 900 °C, resulting in prominent age hardening of (Ti,Al)N is in good agreement to the temperature at the cutting edge of a cutting tool insert during metal machining, e.g., in a turning operation [13]. In addition, high stresses co-exist at the cutting edge during metal machining [14]. Recently, we have shown that a combination of high temperature and high stresses influence the evolving microstructure and phase stability of (Ti,Al)N during decomposition [15,16]. By *ab-initio* calculations, Alling et al. [17] propose that the application of a high hydrostatic pressure promotes coherent isostructural decomposition of (Ti,Al)N stabilizing the c-AlN phase over the less favorable w-AlN phase. Similar ideas have also been proposed by Holec et al. [18].

To date, substantial efforts have been focused on the thermal and physical properties as well as the performance of $Ti_{1-x}Al_xN$ coatings whereas the actual details of the spinodal decomposition process have drawn limited attention, especially in the situation of a real cutting application at high temperatures and high pressures. Studies on c-$Ti_{0.34}Al_{0.66}N$-based monolithic and multilayer systems by applying different thermal anneal sequences have demonstrated the presence of the anticipated decomposition products with a strong elemental

* Corresponding author at: Nanostructured Materials, Department of Physics, Chemistry and Biology, IFM, Linköping University, SE-58183 Linköping, Sweden.
E-mail address: matjo@ifm.liu.se (M.P. Johansson Jõesaar).

0257-8972
http://dx.doi.org/10.1016/j.surfcoat.2013.07.031

partitioning between the c-AlN and c-TiN rich domains, see e.g. [3,5]. Similar results have also been verified by 3D atom probe tomography of monolithic (Ti,Al)N layers [19,20]. In addition, the final decomposition stage demonstrating a dual c-TiN and w-AlN phase structure has also been discussed [2,21]. However, only a few experimental studies focuses on phenomena occurring at an earlier stage of (Ti,Al)N decomposition [20,22]. By means of analytical transmission electron microscopy (TEM), here are presented new insights on the initial stage of the spinodal decomposition process in cathodic arc evaporated cubic $Ti_{1-x}Al_xN$ layers where x = 0.31, 0.37, 0.47 and 0.66, i.e., solid solution compositions with significantly different elastic anisotropy [10] and positioned differently inside the miscibility gap [9]. The local microstructure and chemistry of c-$Ti_{1-x}Al_xN$ layers after heat treatment are compared to layers exposed to the harsh conditions during metal cutting and discussed with reference to microstructural anisotropy effects, age hardening effects, spinodal decomposition theory and metal cutting performance.

2. Experimental details

Monolithic c-$Ti_{1-x}Al_xN$, x = 0.31, 0.37, 0.47 and x = 0.66, layers were deposited onto blanks (ISO SNUN120408) and turning inserts (ISO TPUN160308 and ISO TNGN110308S-01525) by cathodic arc evaporation using a commercial Sulzer-Metaplas MZR323 coating system. About 2 μm thick layers were grown in 99.995% pure N_2 from composite TiAl cathodes with a composition resulting in the above layers on inserts placed of a rotating fixture held at a bias of −40 V and a temperature of ~450 °C resulting in 100 preferentially oriented (Ti,Al)N layers. More details on the deposition process can be found elsewhere [1–3].

Post deposition isothermal annealing was performed at T_{max} between 700 and 1000 °C in an argon atmosphere at atmospheric pressure using a Sintervac furnace from GCA Vacuum Industries. The temperature was initially increased at a rate of 7 °C/min up to 40 °C below T_{max} and then at a rate of 5 °C/min until T_{max} was reached after which the samples were held isothermally for 2 h and finally allowed to cool down. In addition, small sample pieces ($1.7 \times 0.5 \times 0.5$ mm^3) from selected samples were annealed in vacuum (base pressure $<3 \times 10^{-5}$ torr) using a heating rate of 20 °C/min up to T_{max} and held isothermally for 10 min [16].

Cutting tests for microstructure analysis were performed by continuous turning in a case hardened steel (16MnCr5, 58-62 HRC, case depth 1.2 mm) at a cutting speed v_c = 200 m/min, feed f = 0.15 mm/rev and depth of cut a_p = 0.25 mm for up to 10 min. At the above cutting conditions, a temperature of about 850 °C and a pressure of about 1.8 GPa was obtained at the cutting edge when evaluated according to the methods described elsewhere [13,23].

The microstructure evolution and local compositional variations of as-deposited and worn layers, i.e., in samples obtained close to the tool–chip interface, were characterized by analytical TEM, electron diffraction and scanning TEM (STEM) using a FEI Technai G^2 TF 20 UT operated at 200 kV and equipped with an EDX detector. STEM micrographs were obtained by a high angle annular dark field detector. Elemental mapping was performed using the Technai TIA software. Cross-sectional TEM specimens from the cutting zone, i.e., at the tool–chip interface located ~20 μm from the cutting edge of the insert rake face were prepared using a Zeiss 1540 EsB CrossBeam FIB by the so-called lift-out technique [24].

Selected area electron diffraction patterns (SADP) were analyzed using the Gatan DigitalMicrograph™ software with the DiffTools: Electron Diffraction Software Tools package installed [25]. The diffracted intensities were rotationally averaged about the SADP center and a Radial distribution function (RDF) created with its radial intensity profile on the y-axis and the scattering vector on the x-axis.

Nanoindentation was performed using a UMIS Nanoindentation system equipped with a Berkovich diamond tip. Approximately 40 indents with a maximum load of 30 mN were made on polished tapered cross sections (taper angle ≈ 10°) in as-deposited and post-annealed samples. The hardness, H, was evaluated according to the Oliver and Pharr method [26] and the average hardness values and their standard deviation are reported here. In between measurements, a reference sample of fused silica was indented at the same indentation depth as for the films.

3. Results and discussion

Analytical TEM and STEM in combination with EDX elemental mapping were employed to study c-$Ti_{1-x}Al_xN$ layers in its as-deposited state, after thermal annealing and metal cutting. Fig. 1 shows cross-sectional TEM micrographs with corresponding SADP of 1(a) the c-$Ti_{0.34}Al_{0.66}N$ layer in as-deposited state, 1(b) a middle section of the c-$Ti_{0.34}Al_{0.66}N$ layer after post heat treatment at 900 °C for 2 h and 1(c) a middle section of the c-$Ti_{0.34}Al_{0.66}N$ layer after 10 min of turning operation. Arrows show the crystallographic orientation of the c-$Ti_{0.34}Al_{0.66}N$ lattice, valid for all images 1(a–c). In agreement to a previous study [2], the as-deposited c-$Ti_{0.34}Al_{0.66}N$ layer 1(a) exhibits a defect rich, polycrystalline material with a dense and columnar microstructure. A columnar microstructure is also observed for the post annealed sample 1(b), although with a dramatically reduced defect density due to annihilation of crystal defects during the anneal sequence and observed as much more well-defined columns in the image. Finally and as shown in Fig. 1(c), defect annihilation also takes place in the sample after turning, however, not to the same extent as observed after annealing most likely due to the shorter time during turning compared to the annealing sequence. Similar results have recently been obtained in a previous study [15], comparing as-deposited samples with a $Ti_{0.63}Al_{0.37}N$ composition after metal cutting and heat treatments.

Fig. 2 shows the RDF for all SADP's in Fig. 1(a–c). In addition to the solid solution cubic $Ti_{0.34}Al_{0.66}N$ structure, the asymmetric shape of the RDF peaks at about 0.45, 0.5 and 0.7 Å^{-1} indicate the presence of the anticipated decomposition products of both c-AlN and c-TiN phases. Smaller amounts of c-AlN and c-TiN are observed for the as-deposited layer. The layers after post heat treatment and turning reveal a clear contribution of the hexagonal w-AlN phase as indicated by the

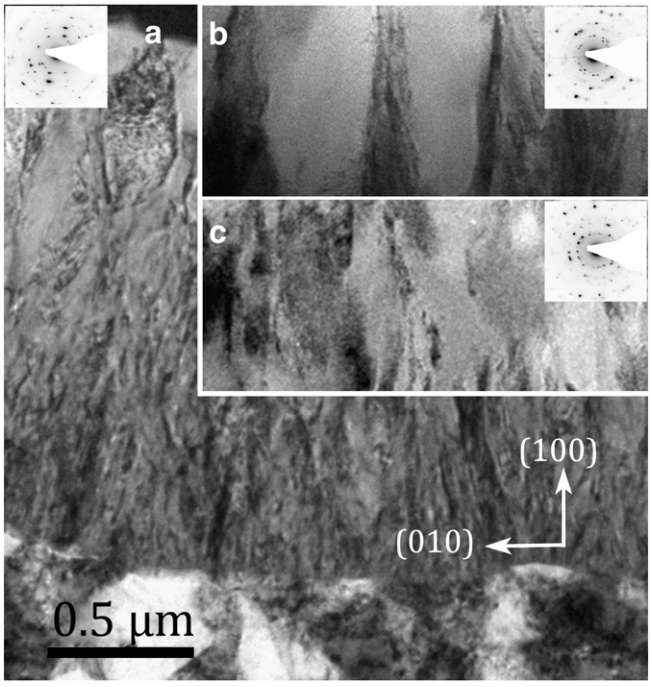

Fig. 1. Bright field cross-sectional TEM images with corresponding selected area diffraction pattern, SADP, of c-$Ti_{0.34}Al_{0.66}N$ in (a) as-deposited state, (b) post heat treatment at 900 °C for 120 min in Ar atmosphere, (c) after 10 min of turning.

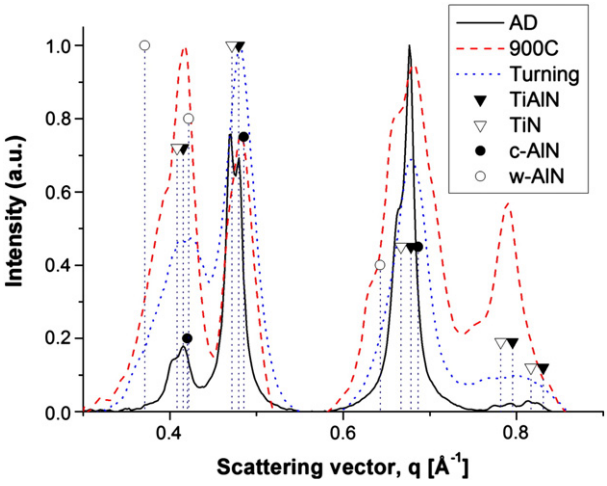

Fig. 2. Radial distribution function (RDF) of the SADPs in Fig. 1 (a–c).

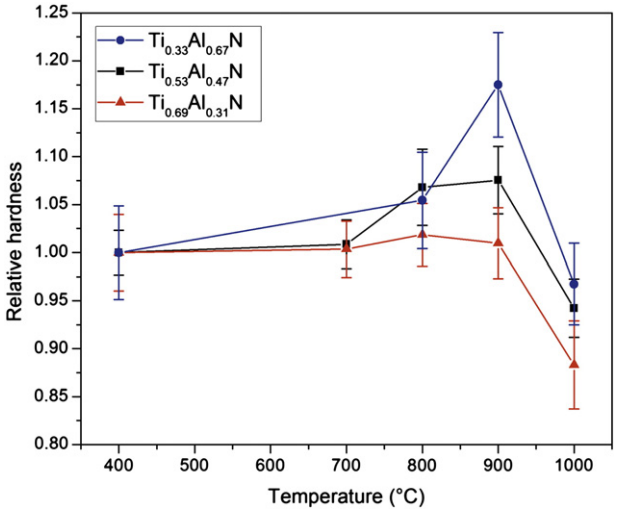

Fig. 3. Hardness relative to as-deposited (400 °C) values for $Ti_{0.69}Al_{0.31}N$, $Ti_{0.53}Al_{0.47}N$ and $Ti_{0.34}Al_{0.66}N$.

asymmetric shape of the peaks at about 0.35 and 0.6 Å^{-1}. The presence of w-AlN in the as-deposited layer cannot be excluded.

The hardness in arc evaporated (Ti,Al)N layers has been discussed in terms of hardening effects resulting from, e.g., small grain size and point defects induced during growth but also in terms of solution and precipitation hardening effects caused by a compositional inhomogeneity of the layers [27]. The same authors also show that the hardness in the as-deposited state of (Ti,Al)N increases with increasing Al content reaching a plateau with an Al content between 50 and 66 at%. In addition, (Ti,Al)N layers typically exhibit age hardening effects at elevated temperatures biased by the decomposition into coherent c-TiN and c-AlN domains [1]. Recently, Rafaja et al. [21] suggested that coherent w-AlN and c-TiN domains present already in the as-deposited state of $Ti_{0.5}Al_{0.5}N$ and dependent on the deposition conditions used have a positive effect on the hardness promoted by a temperature induced decomposition into c-TiN and w-AlN at a low to medium temperatures. A similar idea has also been suggested by Rogström et al. [11] proposing that small domains of w-AlN are formed during the early stages of decomposition. However, at higher Al contents and/or higher temperatures the formation of incoherent w-AlN dominates [2,8] resulting in a degradation of the mechanical properties [2].

In Table 1, the measured hardness values are shown for $Ti_{0.69}Al_{0.31}N$, $Ti_{0.53}Al_{0.47}N$ and $Ti_{0.34}Al_{0.66}N$ in their as-deposited state as well as after a 2 h isothermal anneal at T_{max} = 800, 900 and 1000 °C. As shown, all compositions resulted in an as-deposited hardness of about 30 GPa and a maximum hardness that is obtained after heat treatment at 900 °C whereupon the hardness drops below its as-deposited hardness value. Fig. 3 shows the normalized hardness (against its as-deposited hardness) for each composition as a function of annealing temperature, T_{max}. This plot clearly demonstrates that the coating with the lowest Al concentration $Ti_{0.69}Al_{0.31}N$ only exhibits a small, if any, age hardening effect while for the coatings with higher Al concentrations, $Ti_{0.53}Al_{0.47}N$ and $Ti_{0.34}Al_{0.66}N$ reveal a significant age hardening effect of around 7% and 18%, respectively. The highest hardness is obtained after annealing at T_{max} between 800 and 900 °C. Also, the $Ti_{0.69}Al_{0.31}N$ composition is close to the where $Ti_{1-x}Al_xN$, x = 0.28 is elastically isotropic (anisotropic for $x \neq 0.28$) [10].

Combining the effect of Al content and the application of high temperature high pressure conditions as in the case of a continuous turning operation, the progression of the flank wear during cutting was investigated by Hörling et al. [27]. It was reported that the increasing Al content was associated with a reduction of the flank wear up to the solid solution limit of ~0.7. Although this behaviour follows the observed trends in hardness data the actual mechanism for a higher hardness with higher aluminium content is not clear. The effect of anisotropy on hardening effects, spinodal decomposition and cutting performance will further be discussed below.

According to the spinodal decomposition theory [28,29], the initial stage of the decomposition of a solid solution is characterized by a periodic and highly oriented modulation of two coherent phases resulting in concentrations waves along elastic compliant crystal direction [28] of the material. In a cubic system, the elastically soft directions can be correlated to the Zener's anisotropy factor $A = 2C_{44}/(C_{11} - C_{12})$ [30] for which A < 1 and A > 1 predicts concentration waves along <111> and <100> directions, respectively [28]. In the case of $Ti_{1-x}Al_xN$, recent *ab-initio* calculations [10] have demonstrated a strong correlation between the Al content, x, and the anisotropy factor where $A \geq 1$ for $x \geq 0.28$ and hence predicts concentration waves along <100> crystal directions [28].

TEM was employed to study the elemental partitioning between the phases as well as the orientation of the concentration waves during the decomposition of c-$Ti_{0.34}Al_{0.66}N$ coatings engaged in a metal cutting application. Fig. 4(a) shows a bright field TEM (BF-TEM) micrograph obtained from an FIB cross section of turning insert close to the cutting edge after a 5 min of metal cutting operation. The figure shows a cross-sectional view of the top portion of the c-$Ti_{0.34}Al_{0.66}N$ coating, adhered work piece residue, WPR, material remnant from the cutting process and the Pt protection layer originating from the FIB sample fabrication. The WPR and Pt layers will not be addressed in this work. Overall, the c-$Ti_{0.34}Al_{0.66}N$ layer reveals a columnar micro structure. In more detail, the presence of c-AlN and c-TiN-rich domains, as a result of the ongoing decomposition process, can be identified within the columnar grains and imaged with brighter and darker image contrast. Fig. 4(b) shows a higher magnification BF-TEM micrograph from the middle part of the column that in Fig. 4(a) is imaged with a brighter contrast. Arrows show the crystallographic orientation of the c-$Ti_{0.34}Al_{0.66}N$ lattice. Here, the spinodal decomposition waves and the orientation of the underlying crystal lattices are observed simultaneously.

Table 1
Hardness vs. composition and annealing temperature.

Annealing temperature [°C]	$Ti_{0.69}Al_{0.31}N$ [GPa]	$Ti_{0.53}Al_{0.47}N$ [GPa]	$Ti_{0.34}Al_{0.66}N$ [GPa]
a.d.	33.1 ± 1.3	33.6 ± 0.80	31.4 ± 1.5
800	33.7 ± 1.0	35.9 ± 1.3	33.1 ± 1.6
900	33.4 ± 1.1	36.1 ± 1.2	36.9 ± 1.7
1000	29.2 ± 1.5	31.7 ± 1.0	30.4 ± 1.3

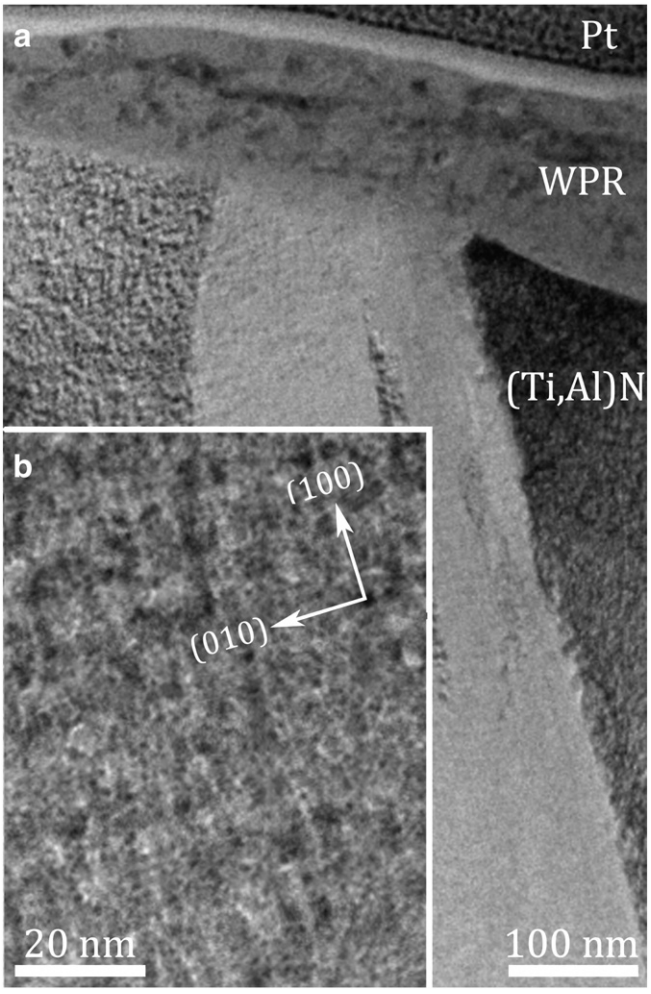

Fig. 4. High resolution TEM of c-$Ti_{0.34}Al_{0.66}N$ after turning obtained (a) close to the top surface including the WPR and Pt layers and (b) a higher magnification image of the middle column obtained close to the [001] zone axis in (a).

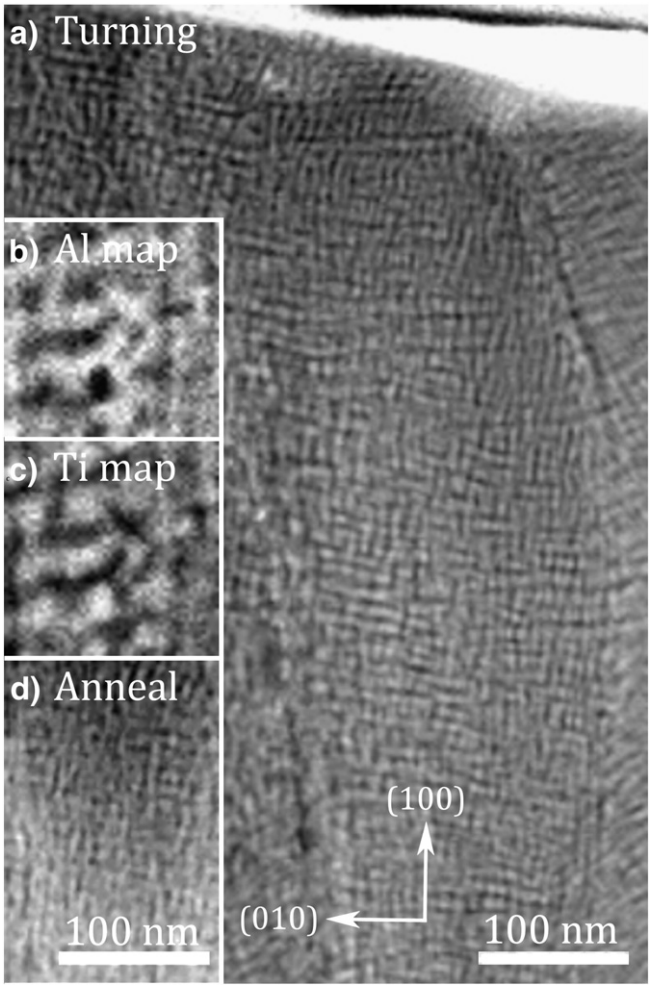

Fig. 5. Higher-magnification STEM images of c-$Ti_{0.34}Al_{0.66}N$ (a) after 10 min of turning, (b–c) corresponding Al and Ti STEM-EDX elemental maps, respectively after turning and (d) after heat treatment at 900 °C for 120 min.

To further enhance the elemental partitioning between c-AlN and c-TiN rich domains STEM was applied to study the details of the decomposition in post heat treated and machined $Ti_{0.34}Al_{0.66}N$ layers. Fig. 5 shows (a) a STEM image from a c-$Ti_{0.34}Al_{0.66}N$ layer after 5 min turning, (b–c) EDX Al- and Ti-elemental maps, respectively, over a 50 × 50 nm^2 area in (a), and (d) a STEM image from a c-$Ti_{0.34}Al_{0.66}N$ layer after post heat treatment at 900 °C. Arrows show the crystallographic orientation of the c-$Ti_{0.34}Al_{0.66}N$ lattice, valid for all images 5(a–d). The Al- and Ti-elemental maps (Fig. 5(b–c)) show a clear elemental partitioning between the c-AlN and c-TiN rich domains. Overall, the decomposed microstructure in Fig. 5(a) shows an interconnected array of the c-AlN (dark contrast) and c-TiN (bright contrast) rich domains with a modulation wavelength of about 10 nm. This microstructure, i.e., both the alignment along elastic compliant <100> directions as well as modulation with a wavelength of the same order is similar between layers exposed to metal cutting and thermal treatment (c.f. Fig. 5(d)). Both Figs. 4 and 5 demonstrates that the composition modulations propagate along elastically soft <100> directions, which is in good agreement with the prevailing spinodal decomposition theory [28].

For comparison, Fig. 6 shows the microstructure of the low Al-containing $Ti_{0.63}Al_{0.37}N$ alloy after (a) metal cutting for 10 min in a carbon steel and (b) 10 min of heat treatment at 1000 °C. Arrows show the crystallographic orientation of the c-$Ti_{0.34}Al_{0.66}N$ lattice. As for $Ti_{0.34}Al_{0.66}N$, the decomposed microstructures have evolved also for $Ti_{0.63}Al_{0.37}N$ during both heat treatment and metal cutting. The domains are of the same size after both metal cutting and heat treatments. The interesting aspect here is however the difference in geometric shape of the domains. As can be seen, the domains in the $Ti_{0.63}Al_{0.37}N$

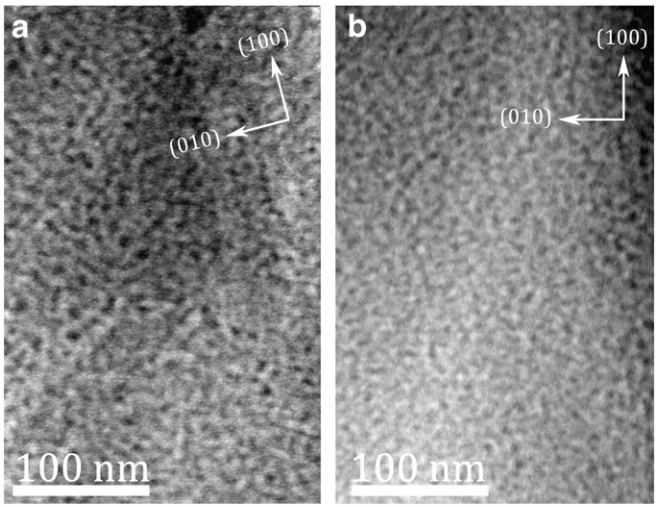

Fig. 6. STEM images of c-$Ti_{0.63}Al_{0.37}N$ after a) 10 min of turning and b) after post heat treatment at 1000 °C for 10 min.

are not aligned along specific directions, as is the case for $Ti_{0.34}Al_{0.66}N$, resulting in a more randomly ordered microstructure. The reason behind this effect is attributed to the decrease in Al content itself and the corresponding decrease in elastic anisotropy [10]. Moreover, this effect would probably be even more apparent at Al concentrations closer to the isotropic composition at $x = 0.28$ [10]. Although an applied stress during the decomposition of (Ti,Al)N coatings is known to affect the directionality of the evolving microstructure [30], no or very weak tendency for such behavior is observed during the metal cutting experiment (c.f. Fig. 6(a)).

The different microstructures in $Ti_{0.63}Al_{0.37}N$ and $Ti_{0.34}Al_{0.66}N$ will result in different strengthening. Sonderegger and Kozeschnik [31] discussed the geometrical effect of particle strengthening in face-centred cubic crystals and pointed out two major microstructural features that link to macroscopic mechanical properties of the material, i.e. the distance between the particles (domains) and their geometrical shape. In our case the $Ti_{0.34}Al_{0.66}N$ alloy basically consists of c-TiN rich ellipsoidal domains in coherently embedded in an AlN-rich matrix (majority phase) while in the $Ti_{0.63}Al_{0.37}N$ alloy the situation is the opposite with spherical AlN-rich domains coherently embedded in a TiN-rich matrix (majority phase). The coherency between c-TiN and c-AlN domains for these materials has previously been shown by, e.g., Knutsson et al. [32]. Following the arguments by Sonderegger and Kozeschnik [31] an enhanced strengthening should occur for elongated domains ($Ti_{0.34}Al_{0.66}N$) compared to the more spherical situation ($Ti_{0.63}Al_{0.37}N$). Hence we conclude that the observed hardness enhancement observed in our work and in several publications [27,33–37] with Al-content is related to the more pronounced elongated domain shape with increasing Al-content.

We note that the tribological situation at the cutting edge is more complex than a laboratory hardness indent and other wear mechanisms than plastic deformation may determine the lifetime of a tool. However, since the observed lifetime of TiAlN-coated cutting inserts often seems to scale with hardness [27] we propose its origin to be the differences in evolving microstructures for different compositions, as discussed above.

4. Conclusions

We have characterized layers with a different elastic anisotropy using electron microscopy after heat treatments and metal cutting. We have observed the early stages of spinodal decomposition after minutes of cutting in combination with traces of w-AlN. A strong alignment along elastically soft <100> directions is observed for $Ti_{0.34}Al_{0.66}N$ layers in accord with spinodal decomposition theory. With a composition closer to the isotropic limit ($Ti_{0.63}Al_{0.37}N$) the evolving microstructure instead shows domains with random alignments. Hardness measurements show a minute age hardening close to the isotropic limit whereas the most anisotropic microstructure reveals an age hardening of about 18%. We therefore conclude that the microstructure during the spinodal decomposition is not only affected by the relative amount of metal Ti/Al ratio in $Ti_{1-x}Al_xN$ but also highly dependent on the elastic anisotropy which is a probable explanation to the previous shown wear resistance scaling with Al composition.

Acknowledgements

The Swedish Foundation for Strategic Research (SSF) projects Designed multicomponent coatings, Multifilms and the strategic mobility 2009 project SM09-0033 are gratefully acknowledged for financial support.

References

[1] P.H. Mayrhofer, A. Hörling, L. Karlsson, J. Sjölen, T. Larsson, C. Mitterer, L. Hultman, Appl. Phys. Lett. 83 (10) (2003) 2049.
[2] A. Hörling, L. Hultman, M. Odén, J. Sjölen, L. Karlsson, J. Vacuum Sci. Technol. A Vacuum, Surf., Films 20 (5) (2002) 1815.
[3] A. Knutsson, M.P. Johansson, P.O.A. Persson, L. Hultman, M. Odén, Appl. Phys. Lett. 93 (14) (2008) 143110.
[4] D. McIntyre, J.E. Greene, G. Hakansson, J.E. Sundgren, W.D. Munz, J. Appl. Phys. 67 (3) (1990) 1542.
[5] A. Knutsson, M.P. Johansson, L. Karlsson, M. Odén, J. Appl. Phys. 108 (4) (2010) 044312, (7 pp.).
[6] O. Knotek, M. Bohmer, T. Leyendecker, J. Vacuum Sci. Technol. A Vacuum, Surf., Films 4 (1986) 2695.
[7] A. Knutsson, M.P. Johansson, L. Karlsson, M. Odén, Surf. Coat. Technol. 205 (16) (2011) 4005.
[8] F. Adibi, I. Petrov, L. Hultman, U. Wahlström, T. Shimizu, D. McIntyre, J.E. Greene, J.E. Sundgren, J. Appl. Phys. 69 (9) (1991) 6437.
[9] B. Alling, A.V. Ruban, A. Karimi, O.E. Peil, S.I. Simak, L. Hultman, I.A. Abrikosov, Phys. Rev. B Condens. Matter Mater. Phys. 75 (4) (2007) 45123.
[10] F. Tasnadi, I.A. Abrikosov, L. Rogstrom, J. Almer, M.P. Johansson, M. Odén, Appl. Phys. Lett. 97 (23) (2010) 231902.
[11] L. Rogström, J. Ullbrand, J. Almer, L. Hultman, B. Jansson, M. Odén, Thin Solid Films 520 (17) (2012) 5542.
[12] J.W. Cahn, Acta Metall. 11 (12) (1963) 1275.
[13] R. M'Saoubi, H. Chandrasekaran, Int. J. Mach. Tools Manuf. 44 (2-3) (2004) 213.
[14] K.-. Bouzakis, G. Skordaris, S. Gerardis, G. Katirtzoglou, S. Makrimallakis, M. Pappa, E. Lill, R. M'Saoubi, Surf. Coat. Technol. 204 (6-7) (2009) 1061.
[15] N. Norrby, M.P. Johansson, R. M'Saoubi, M. Odén, Surf. Coat. Technol. 209 (2012) 203.
[16] N. Norrby, H. Lind, G. Parakhonskiy, M.P. Johansson, F. Tasnádi, L.S. Dubrovinsky, N. Dubrovinskaia, I.A. Abrikosov, M. Odén, J. Appl. Phys. 113 (5) (2013) 053515.
[17] B. Alling, M. Oden, L. Hultman, I.A. Abrikosov, Appl. Phys. Lett. 95 (18) (2009) 181906.
[18] D. Holec, F. Rovere, P.H. Mayrhofer, P.B. Barna, Scr. Mater. 62 (6) (2010) 349.
[19] L.J.S. Johnson, M. Thuvander, K. Stiller, M. Odén, L. Hultman, Thin Solid Films 520 (13) (2012) 4362.
[20] R. Rachbauer, E. Stergar, S. Massl, M. Moser, P.H. Mayrhofer, Scr. Mater. 61 (7) (2009) 725.
[21] D. Rafaja, C. Wüstefeld, C. Baehtz, V. Klemm, M. Dopita, M. Motylenko, C. Michotte, M. Kathrein, Metall. Mater. Trans. A 42 (3) (2011) 559.
[22] R. Rachbauer, S. Massl, E. Stergar, D. Holec, D. Kiener, J. Keckes, J. Patscheider, M. Stiefel, H. Leitner, P.H. Mayrhofer, J. Appl. Phys. 110 (2) (2011) 023515.
[23] H. Chandrasekaran, A. Thuvander, Mach. Sci. Technol. 2 (2) (1998) 355.
[24] A. Flink, R. M'Saoubi, F. Giuliani, J. Sjölen, T. Larsson, P.O.A. Persson, M.P. Johansson, L. Hultman, Wear 266 (11–12) (2009) 1237.
[25] D.R.G. Mitchell, Microsc. Res. Tech. 71 (8) (2008) 588.
[26] W.C. Oliver, G.M. Pharr, J. Mater. Res. 7 (6) (1992) 1564.
[27] A. Hörling, L. Hultman, M. Oden, J. Sjölen, L. Karlsson, Surf. Coat. Technol. 191 (2–3) (2005) 384.
[28] J.W. Cahn, Acta Metall. 10 (3) (1962) 179.
[29] J.W. Cahn, J. Chem. Phys. 42 (1) (1965) 93.
[30] C.M. Zener, Elasticity and Anelasticity of Metals, University of Chicago Press, 1948.
[31] B. Sonderegger, E. Kozeschnik, Scr. Mater. 66 (1) (2012) 52.
[32] A. Knutsson, J. Ullbrand, L. Rogström, N. Norrby, L.J.S. Johnson, L. Hultman, J. Almer, M.P. Johansson Jöesaar, B. Jansson, M. Odén, J. Appl. Phys. 113 (21) (2013) 213518.
[33] A.E. Santana, A. Karimi, V.H. Derflinger, A. Schütze, Mater. Sci. Eng., A 406 (1–2) (2005) 11.
[34] A.E. Santana, A. Karimi, V.H. Derflinger, A. Schütze, Tribol. Lett. 17 (2004) 689.
[35] X. Zhou, A. Wu, W. Qu, X. Jiang, Rare Met. 31 (2012) 178.
[36] A. Kimura, H. Hasegawa, K. Yamada, T. Suzuki, Surf. Coat. Technol. 120–121 (1999) 438.
[37] S. PalDey, S.C. Deevi, Mater. Sci. Eng., A 342 (1–2) (2003) 58.